16th ICAAR LISBOA 2020-2022

16th International Conference on
Alkali-Aggregate Reaction in Concrete
Lisboa | LNEC | Portugal | 31 May - 2 June 2022

http://icaar2020-2022.lnec.pt

Effect of alkali-silica reaction on aggregate interlock shear transfer in reinforced concrete structures

Francis Thériault [(1)], Martin Noël [(2)], Leandro Sanchez [(3)]

(1) University of Ottawa, Ottawa, Canada, ftheriault@l2cexperts.com

(2) University of Ottawa, Ottawa, Canada, MartinNoel@uOttawa.ca

(3) University of Ottawa, Ottawa, Canada, Leandro.Sanchez@uOttawa.ca

Abstract

It is well-known that damage associated with alkali-silica reaction (ASR) in concrete leads to a reduction in mechanical properties such as stiffness and strength. Despite this, the structural consequences of ASR in reinforced concrete structures are still not clear. This is in large part due to the complex stress states that develop as a result of restrained expansion, a phenomenon often referred to as chemical prestressing. The relative contribution of these competing factors have been the subject of considerable debate. The present study aims to improve understanding of the effect of ASR on aggregate interlock shear transfer by decoupling the prestressing effect from the damaged response. Eight pre-cracked shear push-off specimens were constructed with dimensions of 670 mm x 400 mm x 120 mm using reactive coarse aggregates. For each expansion level (0.00%, 0.04%, 0.07% and 0.12%), two specimens were fabricated: one was reinforced internally and placed in an environmental chamber until the desired expansion level was reached, and a companion specimen containing lithium (to inhibit ASR development) was externally reinforced and mechanically prestressed to achieve the same confining normal stress across the shear crack plane. The push-off tests were conducted under displacement control and the crack kinematics were closely monitored. The experimental results were compared to various analytical models for aggregate interlock reported in the literature. The results of this study suggest that although prestressing reduced the initial crack width, it did not significantly affect the crack dilation behaviour during loading nor the maximum shear strength obtained. It was also observed that ASR microcracks in damaged coarse aggregates reduced the shear crack roughness and resulted in reductions in the aggregate interlock shear strength of up to nearly 30%. Further testing is recommended to extend the results to other aggregate types, expansion levels, and confinement conditions.

***Keywords**: aggregate interlock; alkali-silica reaction; chemical prestressing; RC; shear behaviour*

1. INTRODUCTION

Alkali-silica reaction (ASR) is a physicochemical process that takes place between the alkali hydroxides from the concrete pore solution (Na+, K+, and OH-) and some siliceous mineral phases present in the coarse and fine aggregates used to make concrete. ASR generates a “secondary” product (i.e. ASR-gel), that swells upon moisture uptake, leading to microcracking and reductions in mechanical properties of the affected material. ASR has been reported to significantly reduce the service life of RC structures worldwide [1-3].

The chemical reaction and the physical process associated with ASR have been studied extensively, but the implications on the serviceability and/or ultimate limit states of affected structures remain unclear. The shear resistance of ASR-affected concrete members, in particular, is not well understood. The formation of cracks within coarse aggregates can potentially reduce the shear stresses resisted by aggregate interlock across a cracked concrete surface. On the other hand, the compressive stresses induced by the so-called chemical prestressing effect have a tendency to increase shear strength. Thus, the net effect of ASR damage on the total shear resistance of concrete members with different geometries, reinforcement, and boundary conditions is not clear. This research aims to decouple the contributions of chemical prestressing (i.e. the increase in normal stresses across the cracked surface) from that of the internal damage caused by ASR by comparing a series of shear push-off test specimens with ASR-induced damage to undamaged specimens subjected to similar levels of normal stress across the critical shear plane. The experimental shear stress-slip relationships are then compared to those predicted by three existing aggregate interlock models.

2. BACKGROUND

2.1 Push-off testing and aggregate interlock

Several researchers have used shear push-off specimens to investigate aggregate interlock behaviour [4-7]. The specimen geometry and loading are intended to avoid bending stresses and obtain a pure shear failure. It is also common to initiate a vertical crack along the shear plane since aggregate interlock is only engaged after a crack has formed [8-10]. Since the crack interface is rough, shear slip is accompanied by crack dilation which induces tensile stress in the reinforcement and compressive stress on the cracked concrete faces. Similar to the friction experienced between any solid material surfaces, with an increase in the normal compressive stress, the aggregate interlock shear friction increases. Researchers have proposed various models to describe aggregate interlock behaviour in concrete. Three well-known models are briefly summarized below.

2.1.1 Walraven and Reinhardt [7]

Walraven & Reinhardt [7] derived a theoretical model that considers aggregates to be perfectly spherical and have a much higher strength and stiffness than the surrounding cement matrix. Thus, the crack goes through the cement matrix and around all aggregates. With applied shear loads, the cement paste deforms and contact areas form between the spherical aggregate particles protruding from one face and the cement matrix from the opposite face. The following relations between shear stress, normal stress, crack slip and crack width were proposed:

$$\tau = -0.04f_c' + \{1.8w^{-0.80} + (0.292w^{-0.707} - 0.25) \cdot f_c'\}\Delta \quad (\tau > 0) \tag{1}$$

$$\sigma = -0.06f_c' + \{1.35w^{-0.63} + (0.242w^{-0.552} - 0.19) \cdot f_c'\}\Delta \quad (\sigma > 0) \tag{2}$$

where τ and σ are the shear and normal stress, respectively, in MPa, w and Δ are the crack width and shear slip, respectively, in mm, and f'$_c$ is the cylinder compressive strength in MPa.

2.1.2 Gambarova and Karakoc [11]

Theoretical results for a constant crack width based on a simplified micromechanics model [12], were compared with test results obtained with constant normal stress. The authors found intersection points between shear stress-displacement curves at constant crack opening values and for constant confinement conditions. For each intersection point, they plotted the four parameters of interest, τ, σ, Δ, and w, in the plane (σ,Δ), and developed the following relationship between normal stress and crack displacements for constant crack opening:

$$\sigma = -a_1 a_2 \frac{\Delta\tau}{(w^2\Delta^2)^q} \tag{3}$$

where $a_1 a_2$ = 0.62 and q = 0.25.

An equation was also proposed for the shear stress that accounts for the effects of aggregate size:

$$\tau = \tau_0 \left(1 - \sqrt{\frac{2w}{D_{max}}}\right) \frac{c_1 r + c_2 r^4}{1 + c_2 r^4} \tag{4}$$

$$r = \Delta / w \tag{5}$$

$$c_1 = \frac{10}{f_c'} \tag{6}$$

$$c_2 = 2.44(1 - 16.33f_c') \tag{7}$$

where D_{max} is the maximum aggregate size in mm and τ_0 represents the shear strength of the crack in the limit case of zero crack opening in MPa.

2.1.3 Li et al. [13]

Li et al. [13] conducted a series of experiments with pre-cracked RC push-off specimens and measured the crack surfaces using a digitizer, which allowed them to model the crack geometry. They proposed that the crack surface is divided into "contact units" of different inclinations and assumed that the directional distribution of the contact units is represented by a stochastic contact density function. The simplified equations for shear and normal stresses were calculated by analytical integration of the contact compressive force with respect to the angle of inclination of the contact units:

$$\tau = 3.83 f_c'^{1/3} \frac{r}{1 + r^2} \tag{8}$$

$$\sigma = 3.83 f_c'^{1/3} \left[\frac{\pi}{2} - \cot^{-1} r - \frac{r}{1 + r^2}\right] \tag{9}$$

Similarly to Equation 4, the above equations relate the stresses to the crack slip-to-width ratio, r. In this case, however, the stresses are independent of the maximum aggregate size.

2.2 ASR and shear

ASR distinguishes itself from other deterioration mechanisms in concrete since microcracks initiate within the aggregates. In the early stages of ASR (i.e., low expansion levels), the formation of microcracks occurs mainly within the reactive aggregates, and the cement paste is barely affected. Eventually, the microcracks reach the cement paste and later form a network of cracks that link together. Sanchez [14] conducted an extensive experimental research study with ASR-affected specimens including many concrete types (i.e., using coarse and fine reactive aggregates of several natures, different strengths, etc.), and found correlations between the level of expansion and the reduction in compressive strength, tensile strength and elastic modulus. At very high expansion levels (0.30%), reductions of up to 80%, 67% and 35% were obtained for the tensile strength, elastic modulus, and compressive strength, respectively. A more detailed presentation of the reductions in those three mechanical properties as a function of ASR development can be found in [15].

Although the consequences of ASR on the mechanical properties of concrete have been extensively investigated, the structural implications of ASR on real structures remain unclear, particularly with respect to shear [16,17]. A number of shear tests were conducted on ASR-damaged RC slabs without shear reinforcement, but the results are conflicting: [18] observed an increase in capacity of the order of 10%; [19] observed no significant effect on punching shear resistance at moderate levels, but obtained reductions of up to 30% for specimens with high expansion level (0.6%); [20] experienced no significant decrease; and [21] obtained strength reductions of up to 25%.

According to [22], beams affected by ASR with a transverse reinforcement ratio of at least 0.2% do not show a significant decrease in shear capacity, and may even gain strength due to the prestressing effect caused by restrained expansion. Increases in shear strength and reduced deflections for beams were obtained by some researchers [23-25]. Inoue et al. [26] reported that beams with a 1.74% longitudinal reinforcement ratio resulted in a shear failure for sound concrete and flexural failure for damaged concrete, while beams with reinforcement ratios of 0.77 and 1.20% exhibited a bending failure mode for both types of concrete. This demonstrates the beneficial effect of the presence of longitudinal reinforcement on the shear capacity of RC flexural members affected by ASR. Even in cases of large ASR degradation, no reduction in shear strength was experienced by [27] with beams and by [28] with large-scale bent cap beam specimens. On the other hand, for beams without stirrups, both increases and decreases (up to 20%) in shear resistance have been obtained [22].

Aggregate interlock behaviour is also influenced by crack geometry, which can be greatly affected by ASR damage. The weakest link in concrete is generally the ITZ, which is why cracks usually go through the paste outlining the aggregate particles. If a crack intersects several aggregate particles, the roughness of the crack is reduced, the crack opening path is steeper (i.e., large shear displacement compared to crack opening) and aggregate interlock is reduced. Simulating the effect of aggregate splitting in numerical models, [17] obtained reductions in shear capacity of up to 50% in RC beams.

Given the conflicting results available in the literature, there is a need for a mechanistic approach to understand the relative contributions of ASR damage and confinement stresses on shear behaviour of RC. This study presents a step towards that objective.

3. EXPERIMENTAL PROGRAM

3.1 Specimen design

The test program was comprised of eight pre-cracked shear push-off specimens with dimensions of 670 mm x 400 mm x 120 mm (Figure 3.1). Four different expansion levels were considered: 0.00%, 0.04%, 0.07% and 0.12%. For each expansion level, two specimens were fabricated: one with internal reinforcement and the other with external reinforcement. The internally reinforced specimens were used to evaluate the simultaneous effect of the two coupled ASR-induced phenomena on aggregate interlock, while the externally reinforced specimens were designed to isolate the effect of chemical prestressing (i.e. without internal cracking). The details of all the specimens are summarized in Table 3.1.

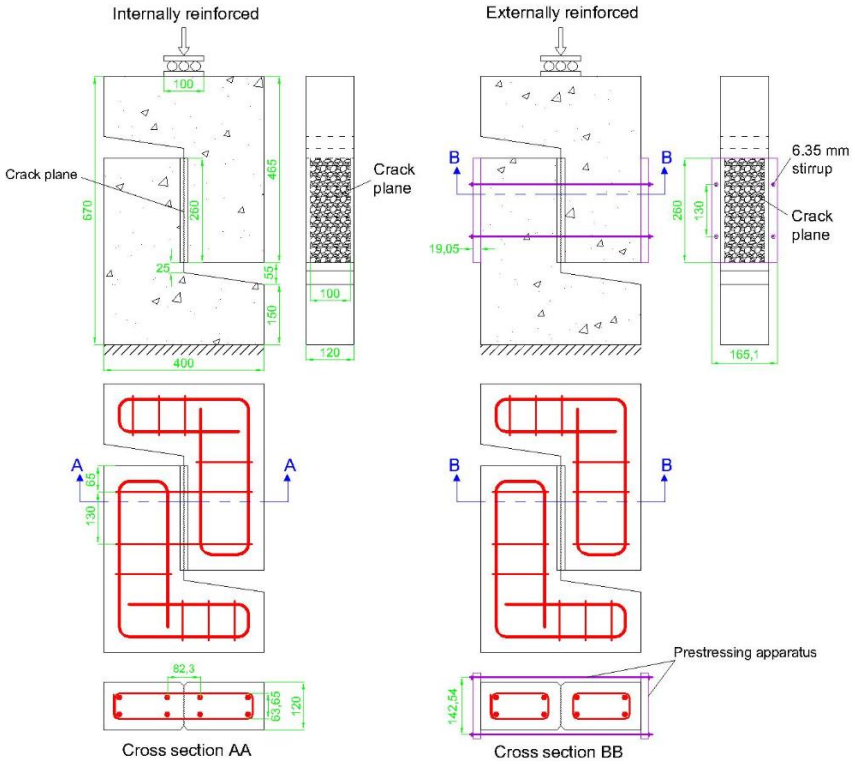

Figure 3.1: Layout of internally and externally reinforced push-off specimens (all dimensions in mm).

Table 3.1: Test program

ID	ρ	Reinforcement across the shear plane	Concrete mix type	ε_{ASR}	Mechanical prestressing strain
00I	0.487%	Internal	Non-reactive	0.00%	0.00%
04I			Reactive	0.04%	
07I			Reactive	0.07%	
012I			Reactive	0.12%	
00E		External	Non-reactive	0.00%	0.005%*
04E					0.04%
07E					0.07%
012E					0.12%

*A slight force was applied to ensure that the prestressing apparatus stayed in place during the test.

The specimens are each labelled with an identifying code. The first two digits correspond to the level of mechanical or chemical prestressing induced across the shear plane (e.g. 04 = 0.04% tensile strain in the stirrups), and the following letter indicates whether the stirrups were internal or external (I = Internal, E = External). The reinforcement ratio of 0.487% corresponds to two smooth double-legged steel stirrups for a total of four 6.35 mm legs crossing the 260 x 100 mm shear plane. In order to reduce dowel action in the internally reinforced test specimens, the 6.35 mm steel bars were passed through circular PVC tubes with a length of 120 mm (Figure 3.2), disrupting their bond with the concrete.

3.2 Materials

3.2.1 Concrete

The two concrete mixtures used in this program were basically the same, except for the use of two ingredients, sodium hydroxide (NaOH) and a lithium-based admixture, which were used to develop and inhibit ASR development, respectively (Table 3.2). NaOH pellets were dissolved in the mix water of the

reactive mixture to raise the total alkali content of the cement and concrete to 1.25% Na_2O_{eq} and 5.25 kg/m^3, respectively. In the case of the control non-reactive mix, NaOH was replaced by a 30%-solid lithium nitrate ($LiNO_3$) solution, at a dosage corresponding to 125% of the "standard dosage" recommended by the manufacturer. For all specimens, a cement content of 420 kg/m^3 was selected in accordance with the requirements of ASTM C 1293-05. A general use Portland cement (equivalent with ASTM Type I) with an alkali content of 0.94% Na_2O_{eq} was used. Springhill greywacke, a highly reactive coarse aggregate (ASTM C 1260 accelerated mortar bar expansion of 0.463% at 14 days in a 1M NaOH solution [29]), was selected. Before its use, it was sieved in order to obtain equal proportions of particles between 4.75 to 9.5 mm, 9.5 to 12.5 mm, and 12.5 to 19 mm. A natural non-reactive sand with a fineness modulus of 2.8 was used in the concrete mixtures. An effective water-to-cement ratio of 0.44 was selected, which corresponds to a theoretical compressive strength of about 35.0 MPa.

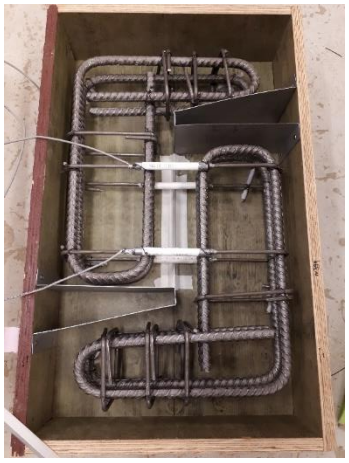

Figure 3.2: Reinforcement cage with PVC tubes installed on the legs of the stirrups

Table 3.2: Concrete mix designs for the reactive and non-reactive specimens

Type of mixture	Cement (kg/m^3)	Fine aggregate (SSD) (kg/m^3)	Coarse aggregate (SSD) (kg/m^3)	Hydration water (kg/m^3)	Water-to-cement ratio	$LiNO_3$ added (L/m^3)	NaOH added (Kg/m^3)	Alkali content (Kg/m^3)
Reactive	420	746	1007	185	0.44	-	1.659	5.25
Non-reactive	420	746	1007	185	0.44	12.36	-	3.965

3.2.2 Steel

Tensile tests were conducted with the steel stirrups to obtain their stress-strain relationship. The elastic modulus was determined to be 200 000 MPa and the yield stress was 555 MPa.

3.3 Fabrication and conditioning

The push-off specimens were manufactured one by one in horizontal wooden molds on their sides so that the shear plane was vertical. A vibrating table was used to consolidate the concrete. After concrete placement, the specimens were covered and moist cured for two days prior to demolding. The non-reactive concrete was moist cured at room temperature with wet burlap under a plastic sheet for five more days, for a total curing period of 7 days. The reactive specimens were placed inside closed containers with high humidity (> 95%), inside an environmental chamber at 38°C.

The ASR-induced expansion was monitored using a DEMEC digital strain gauge with an accuracy of about ±0.001 mm. Four 50.8 mm-long threaded bolts were used as studs, and were positioned such that the measured expansion corresponded to the central core of the push-off specimens in the direction perpendicular to the shear plane. The studs were inserted deep enough to reach the interior of the steel cage close to the stirrups (i.e., 10 mm away from their center). Therefore, the expansion was assumed to be equal to the tensile strain in the reinforcement. The distance between the studs in each pair was 200 mm. Expansion measurements were taken regularly over several months until the push-off specimens reached the desired expansion levels, at which time they were removed from the conditioning

chamber. Unfortunately, specimen 012I did not achieve the required expansion level in time and was not tested.

3.4 Test setup and procedure

After reaching their target expansion, the reactive push-off specimens were removed from the conditioning chamber and cooled for one day before being tested. The non-reactive push-off specimens and their companion cylinders were tested after 28 days.

3.4.1 Prestressing

The external prestressing apparatus for the non-damaged specimens consisted of two steel plates with a thickness of 19.05 mm and connected by four 6.35 mm steel bars passing through them (**Erro! A origem da referência não foi encontrada.**). The bars crossed the shear plane at the same height as those in the internally reinforced specimens. They were threaded at their ends so that nuts could be tightened using a wrench, thereby pressing the plates against the specimen and creating a normal compressive stress on the shear plane. The unrestrained length of the external stirrups was 438 mm. The desired prestressing strain was achieved by monitoring the strain in the four bars as the nuts were being tightened, with a tolerance of +-0.005%.

3.4.2 Pre-cracking

The push-off specimens were pre-cracked by placing them horizontally in the testing machine and applying line loads to opposite faces of the specimen using triangular steel prisms positioned along the two notches to generate a splitting tensile force. The loads were gradually increased until a crack formed in the shear plane. The crack width was measured using four cable transducers installed on the front and rear faces of the push-off specimens, and the stirrup strain was monitored using strain gauges.

3.4.3 Push-off tests

After pre-cracking the specimens, the shear test was performed in the same testing machine. To ensure that the resultant force at the top of the specimen remained vertical and concentric, it was transferred through three steel rollers. The cross head of the testing machine was lowered under displacement control at a constant speed of 1 mm/min. The applied load was recorded with a load cell above the rollers and was divided by the area of the shear plane to obtain the average shear stress (τ) across the crack. The normal compressive stress (σ) was found by summing the tensile force in each stirrup based on the strain gauge readings, and dividing the total force by the shear plane area. For specimens 04I and 07I, a tensile strain of 0.04% and 0.07% was added to all incremental strain gauge measurements to account for chemical prestressing. The crack width (w) was measured using four horizontal linear cable transducers, and slip (Δ) was measured using two vertical cable transducers (Figure 3.3).

Figure 3.3: Externally reinforced specimen in the testing machine: front (left) and rear view (right)

4. RESULTS AND DISCUSSION

4.1 Crack kinematics

The Δ vs.w curves of the seven push-off tests are presented in Figure 4.1. Specimens 00I and 00E showed high initial crack widths (greater than 0.5 mm), which was expected since these specimens had negligible normal stress acting on the shear plane. The prestressed specimens 04E, 07E and 12E, on the other hand, showed the smallest initial crack widths (less than 0.25 mm). Surprisingly, the smallest of those initial crack widths was that of specimen 04E, which was the least prestressed. Similarly, 07I also showed a larger initial crack width than 04I despite having a larger prestressing force (although the crack started to partially close again once the shear test commenced). These discrepancies may be partially attributable to natural variability of the concrete and the lack of precise control of the crack width during the pre-cracking procedure. The results suggest that even small prestressing forces were sufficient to partially close cracks in the concrete, while modest increases in the prestressing force had little further effect on the initial crack widths.

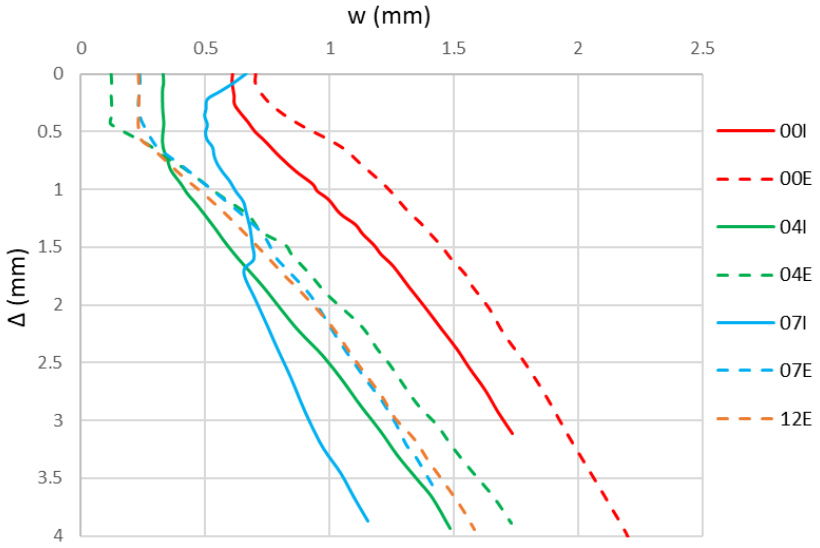

Figure 4.1: Crack slip vs. crack width

The shapes of the Δ vs.w curves were as expected, showing an increase in crack width with shear displacement. Specimen 07I showed a decrease in crack width of almost 0.2 mm at the very beginning of the test, which is potentially attributed to a negative slip that occurred during the pre-cracking phase. The shear cracks started dilating at different slip values; for example, the crack of specimen 00E started opening at a slip as low as approximately 0.1 mm, while the cracks of the other test specimens began to widen at a crack slip varying between 0.3 and 0.6 mm. After the crack width started increasing, until the end of the test, the slope of the Δ vs.w curves either remained constant or increased very slightly. For each test specimen, the average slope of the crack opening path (from the start of the crack widening to a width of 3 mm) is presented in Table 4.1 (in bold). A larger value, corresponding to a steeper slope, indicates that shear slip occurred with relatively little crack dilation. The values in parentheses in Table 3 represent the relative increase or decrease with respect to the slope of 00E or 00I. The slopes of the externally reinforced specimens were all similar, suggesting that mechanical prestressing did not significantly affect crack dilation behaviour.

The slope of 07I was the steepest of all the tests. This agrees with the original expectation that ASR microcracks in the reactive coarse aggregates would likely cause a reduction in crack roughness and thus, a smaller crack dilation during shear displacement. Chemical prestressing may have also contributed to reducing the crack dilation but, as discussed above, no significant effect was experienced from prestressing alone. The crack opening path of 00I was only slightly shallower than 04I, suggesting that the crack roughness is not significantly affected for low levels of expansion.

Table 4.1: Average Δ vs.w curve slopes

Chemical/mechanical prestressing strain (%)	Average Δ vs. w curve slope (mm/mm)		
	Externally reinforced	Internally reinforced	Difference
0.00	**2.31**	**2.55**	+0.24
0.04	**1.98** (-0.33)	**2.81** (+0.26)	+0.83
0.07	**2.54** (+0.23)	**5.90** (+3.35)	+3.36
0.12	**2.36** (+0.05)	N.A	N.A

The values in the last column of Table 3 represent the difference in average crack opening slope between the internally and externally reinforced specimens with equal prestressing (i.e., normal stress before pre-cracking). Since the unbonded length of the internal stirrups, i.e. 130 mm, was smaller than that of the external stirrups, i.e., 438 mm, it was expected that the crack opening paths of the internally reinforced specimens would be steeper. Indeed, a shorter unrestrained stirrup length increases its tensile stiffness (ratio of normal stress to crack width). The difference between the crack opening paths of 00I and 00E was small, was moderate for those of 04I and 04E, and was high for those of 07I and 07E. Considering the previously discussed effects of prestressing and ASR microcracks, these results suggest that the incremental contribution of higher restraint stiffness was relatively small.

4.2 Normal stress vs crack width

Figure 4.2 presents σ vs. w curves for the shear push-off tests. Unfortunately, the normal stress data obtained for specimen 07I had to be omitted since the strain gauge readings were corrupted. The normal stress values appeared to reach a plastic plateau where increases in crack width no longer resulted in a corresponding stress increase. However, the normal stresses never reached 2.73 MPa, which corresponds to the normal stress in the concrete if all four stirrup legs were yielding simultaneously. However, for all tests the width of the shear crack exceeded the theoretical value at which the stirrups should have yielded (calculated by dividing the crack width by the unbonded length of the stirrup legs). For the externally reinforced specimens, the most plausible explanation for this observed response is that the bars yielded in the threaded region at their ends (not captured by the strain gauges). For the internally reinforced specimens, possible explanations include gradual debonding of the smooth bars, stirrup bending caused by dowel forces, pressure on the strain gauges caused by dowel forces, or strain gauge malfunctioning at high strain levels.

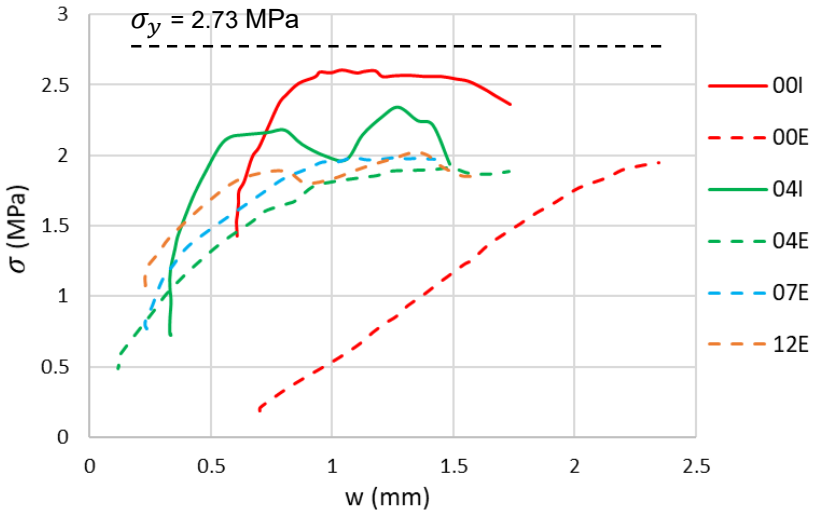

Figure 4.2: Normal stress vs. crack width

As seen in Figure 4.2, since the internal reinforcement provided a higher restraint stiffness than the external reinforcement, higher initial slopes were obtained for the internally reinforced specimens. In

fact, very similar initial slopes were obtained within each series (i.e. internally or externally reinforced). This behaviour was expected, since the strain in the stirrups is proportional to the change in length (crack width) and inversely proportional to the unrestrained length.

The measured maximum normal stresses were higher for the internally reinforced specimens than the externally reinforced specimens, which is believed to be due to yielding of the external stirrups in the threaded end regions. The maximum normal stress was higher for specimen 00I than 04I. Although the reason for this is unclear, it is possible that during loading, the internal reinforcement debonded over a higher length for 04I or that the expansion was actually slightly greater than 0.04% (the value which had to be added to the strain gauge measurements). It is also worth noting that both the initial normal stress and crack width were higher for specimen 00I. For each of the externally reinforced specimens, on the other hand, similar maximum normal stresses of approximately 2 MPa were obtained.

4.3 Shear stress vs crack slip

The shape of the τ vs. Δ curves were as expected, showing a high initial slope followed by a gradual transition to a plastic plateau (Figure 4.3). Most of the specimens showed a stable or gradually decreasing shear stress beyond displacements of approximately 0.5-1.0 mm. Two specimens (i.e., 00E and 07I) presented a gradual increase in shear stress beyond this point such that the maximum shear stress was reached at the end of the test, when the crack width and slip were at their highest.

Higher shear strengths were obtained with the internally reinforced push-off specimens compared to the externally reinforced specimens. This was expected to some extent since the reinforcement stiffness was greater for the internal bars (i.e., shorter unrestrained length), leading to increased normal stresses for a given crack width. Also, the difference could potentially be partially attributed to dowel action of the internal reinforcement, even though efforts were made to prevent it.

Among the internally reinforced specimens, specimen 00I had the highest shear strength, followed by 04I and then by 07I (reductions of 26.6% and 28.6%, respectively). This suggests a decrease in the aggregate interlock shear transfer of RC for increasing ASR expansion levels or, in other words, that the decrease in strength due to ASR microcracks governed over the increase in strength from chemical prestressing for the low confinement levels considered in this study. These decreases were more pronounced than expected and may be at least partially attributable to natural variability in concrete shear strength. The results also suggest that the slope of the Δ-w curve (Figure 4.1) is a better indicator of aggregate interlock strength than the absolute crack width. It is worth noting that Equations 4 and 8 consider the ratio of crack slip to crack width which agrees with this point.

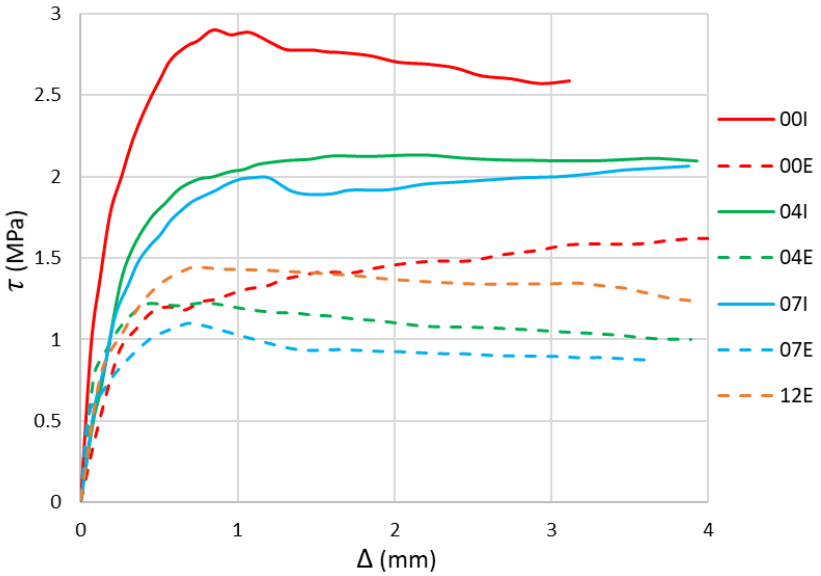

Figure 4.3: Shear stress vs. crack slip

Comparing the τ vs. Δ curves of the externally reinforced specimens, shear strengths ranging from about 1 to 1.5 MPa were obtained, but there was no clear trend between the shear strength and the level of prestressing. It is generally expected that an increase in the initial prestressing (i.e., normal stress) would

enhance the aggregate interlock shear transfer, but this was not consistently observed. These results suggest that for the relatively low levels of confinement and expansion considered in this study, the effect of chemical prestressing was negligible. Increased levels of confinement and/or higher expansion levels may lead to different results.

The shear push-off test results are summarized in Table 4.2. Except for specimen 00E, all of the externally reinforced specimens reached their maximum shear strength at smaller crack slip and width values than the internally reinforced specimens. A reduction in the shear stiffness (initial slope of the τ vs. Δ curves) was also found for the externally reinforced specimens compared to the internally reinforced specimens because of their smaller reinforcement stiffness normal to the crack plane. Among the externally reinforced push-off specimens, an increase in the prestressing force was accompanied by an increase in the measured shear stiffness. For the internally reinforced specimens, the shear stiffness of 04I and 07I were both reduced by 44% compared to the sound specimen 00I, which is likely attributed to a reduced crack roughness due to ASR microcracks.

Table 4.2: Maximum shear and normal stresses obtained in the push-off tests

Chemical/ Mechanical prestressing strain (%)	Internally reinforced					Externally reinforced				
	τ_{max} (MPa)	σ_{max} (MPa)	Δ at τ_{max} (mm)	w at τ_{max} (mm)	Shear stiffness (MPa/mm)	τ_{max} (MPa)	σ_{max} (MPa)	Δ at τ_{max} (mm)	w at τ_{max} (mm)	Shear stiffness (MPa/mm)
0.00	2.90	2.60	0.84	0.86	11.1	1.63	1.94	4.63	2.35	4.21
0.04	2.13	2.35	2.22	0.88	6.15	1.23	1.91	0.81	0.41	9.35
0.07	2.07	N.A	3.87	1.15	6.15	1.10	1.98	0.70	0.35	10.8
0.12	N.A	N.A	N.A	N.A	N.A	1.44	2.02	0.73	0.33	11.4

4.4 Analysis

The shear stress-slip relationships obtained in the push-off tests are compared with those predicted by Equations 1, 4, and 8 in Figure 4.3. The three models produced stress-slip curves of different shapes and with large variations in values. The shape of the Li et al. [13] curves were the closest to those of the experimental results, but the calculated stress values were about two to five times greater than the data from the tests. In fact, with the exception of specimens 00I and 00E, which showed greater shear stresses than those predicted by the model developed by Walraven & Reinhardt [7], the experimental shear stresses were consistently smaller than those predicted with the three models from the literature. This may be partially attributed to the relatively low reinforcement restraint stiffness of the specimens tested in this project. This reduced the normal stress (and thus the shear stress) for given crack displacements, while none of the three simplified shear equations include the normal stress as a parameter. For example, the simplified model of Walraven & Reinhardt [7] was derived from the experimental results of push-off specimens with reinforcement ratios ranging from 0.56% to 2.24%. For a crack width of 0.6 mm, they measured normal stresses ranging from 3.6 to 7.8 MPa. In their shear tests conducted with constant crack openings of 0.1, 0.5 and 1.0 mm, Li et al. [13] measured normal stresses reaching 4 to 5.8 MPa. In this study, the maximum normal stresses obtained ranged from 1.91 to 2.6 MPa. The fact that the three models overpredicted the aggregate interlock shear strength of the push-off specimens tested in this project suggests that the equations may not be suited for lightly reinforced concrete. The difference in strength may also be partially related to the observation that, regardless of the specimen, many coarse aggregates were split by the shear crack resulting in a relatively smooth crack surface.

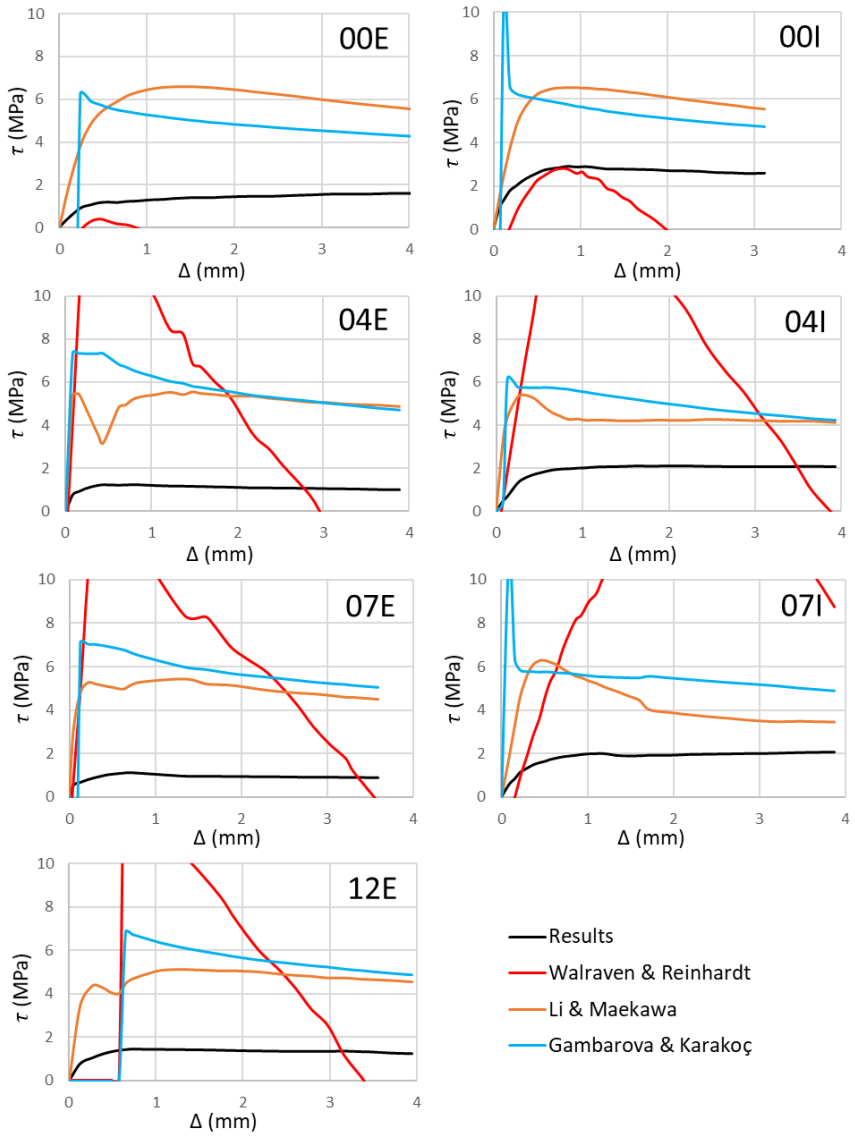

Figure 4.4: Shear-slip behaviour of push-off specimens compared with existing models

Table 4.3 presents the shear strength ratios between the experimental values and those predicted by the three models for a crack slip of 1 mm and for the maximum experimental shear stress. Due to their higher reinforcement restraint stiffness, higher shear stresses were obtained with the internally reinforced specimens, which is why their differences with the predicted shear stresses are smaller than the externally reinforced specimens.

Table 4.3: Experimental to predicted shear strength ratios

Chemical/ mechanical prestressing strain (%)	Experimental to predicted shear strength ratios											
	External reinforcement						Internal reinforcement					
	At 1 mm crack slip			At peak shear stress			At 1 mm crack slip			At peak shear stress		
	W&R	L&M	G&K	W&R	L&M	G&K	W&R	L&M	G&K	W&R	L&M	G&K
0.00	N.A*	0.20	0.24	N.A*	0.31	0.39	1.09	0.44	0.51	1.04	0.44	0.50
0.04	0.12	0.22	0.19	0.11	0.23	0.19	0.14	0.44	0.37	0.23	0.50	0.44
0.07	0.09	0.20	0.17	0.09	0.21	0.16	0.22	0.37	0.36	0.24	0.60	0.42
0.12	0.12	0.28	0.23	0.09	0.31	0.21	N.A					

*The predicted shear stress value was negative and thus removed.

5. CONCLUSIONS

Seven pre-cracked RC push-off specimens were tested to study the effect of low to moderate ASR expansion levels (i.e., 0.04, 0.07 and 0.12%) on aggregate interlock shear behaviour. The simultaneous effects of chemical prestressing and ASR microcracks on the aggregate interlock were decoupled by testing specimens with internal reinforcement and others prestressed with external reinforcement. The following conclusions may be drawn:

- Although prestressing reduced the crack width during the pre-cracking phase, it did not affect the crack dilation behaviour during loading nor the maximum shear strength.
- The steepest crack opening path was obtained for the internally reinforced push-off specimen with an expansion of 0.07%, suggesting that ASR microcracks in damaged coarse aggregates reduced the crack roughness. Shear strength reductions of 26.6 and 28.6% were observed for internally reinforced specimens with expansions of 0.04 and 0.07%, respectively, and their shear stiffness was reduced by 44%. These shear strength reductions were more pronounced than expected, especially for the expansion level of 0.04%.
- For the expansion levels and confinement conditions considered in this study, the decrease in aggregate interlock strength due to ASR microcracks governed over the increase in strength from chemical prestressing.
- Further testing at higher expansion levels and reinforcement ratios are recommended to expand the range of test parameters and lead to the development of rational models.

6. REFERENCES

[1] Thomas, M. D. A., Folliard, K. J., Fournier, B., Rivard, P., & Drimalas, T. (2013). Methods for Evaluating and Treating ASR-Affected Structures: Results of Field Application and Demonstration Projects Volume I: Summary of Findings and Recommendations Final Report.

[2] Sanchez, L., Fournier, B., Bastien, J., & Mitchell, D. (2016). Assessment of Structures Subject to Concrete Degradation.

[3] Thomas, M. D. A., Fournier, B., Folliard, K. J., & Resendez, Y. (2011). Alkali-silica reactivity field identification handbook. FHWA-HIF-12-022, Federal Highway Administration, US Department of Transportation. 80 p.

[4] Fenwick, R. C., & Paulay, T. (1968). Mechanism of Shear resistance of Concrete Beams. Journal of the Structural Division, ASCE, 94(No. ST10), 2235–2350.

[5] Taylor, H. (1970). Investigation of forces carried across cracks in reinforced concrete beams by interlock of aggregates. Cement and Concrete Research, 22.

[6] Wight, J. k. (2016). Shear Friction, Horizontal Shear Trasnfer, and Composite Concrete Beams. In Reinforced Concrete Mechanics and Design (7th ed., pp. 852–872). Pearson Education.

[7] Walraven, J. C., & Reinhardt, H. W. (1981). Theory and Experiments on the Mechanical Behaviour of Cracks in Plain and Reinforced Concrete Subjected to Shear Loading. Heron, 26(1A), 1–68.

[8] Hofbeck, J. A., Ibrahim, I. O., & Mattock, A. H. (1969). Shear Transfer in Reinforced Concrete. ACI Journal, Proceedings, 66(2), 119–128. https://doi.org/10.14359/7349.

[9] Mattock, A. H., & Hawkins, N. M. (1972). Shear Transfer in Reinforced Concrete—Recent Research. Prestressed Concrete Institute, 17(2), 55–75.

[10] Hsu, T. C., Mau, S. T., & Chen, B. (1987). Theory of Shear Transfer Strength in Reinforced Concrete. ACI Structural Journal, 84(2), 149–160. https://doi.org/10.14359/2834.

[11] Gambarova, P. G., & Karakoc, C. (1983). New Approach To the Analysis of the Confinement Role in Regularly Cracked Concrete Elements. In Transactions of the International Conference on Structural Mechanics in Reactor Technology.

[12] Bazant, Z. P., & Gambarova, P. (1980). Rough cracks in reinforced concrete. ASCE J Struct Div, 106(4), 819–842.

[13] Li, B., Maekawa, K., & Okamura, H. (1989). Contact density model for stress transfer across cracks in concrete. Journal of the Faculty of Eng., the University of Tokyo (B), Vol. XL(1), 9–52.

[14] Sanchez, L.F.M. (2014). Contribution to the assessment of damage in aging concrete infrastructures affected by alkali-aggregate reaction. 341.

[15] Sanchez, L.F.M., Fournier, B., Jolin, M., Mitchell, D., & Bastien, J. (2017). Overall assessment of Alkali-Aggregate Reaction (AAR) in concretes presenting different strengths and incorporating a wide range of reactive aggregate types and natures. Cement and Concrete Research, 93, 17–31.

[16] Gowripalan, N., & Cao, J. (2018). Effect of Alkali Silica Reaction on Bond Strength and Load Capacity of Effect of Alkali Silica Reaction on Bond Strength and Load Capacity of Reinforced Concrete Structures. 5th International Fib Congress, October, 3088–3099.

[17] Noël, M., Sanchez, L., & Tawil, D. (2017). Structural implications of internal swelling reactions in concrete: review and research needs. Magazine of Concrete Research, 70(20), 1052–1063. https://doi.org/10.1680/jmacr.17.00383.

[18] Bilodeau, S., Allard, A., Bastien, J., Pissot, F., Fournier, B., Mitchell, D., & Bissonnette, B. (2016). Performance Evaluation of Thick Concrete Slabs Affected by Alkali-Silica Reaction (ASR) - Part II: Structural Aspects. 15th International Conference on Alkali-Aggregate Reaction in Concrete.

[19] Clark, L., & Ng, K. (1989). The Effect of Alkali-Silica Reaction on the Punching Shear Strength of Reinforced Concrete Slabs. 8th International Conference on AAR in Concrete.

[20] Hansen, S. G. (2019). Influence of Alkali-Silica Reaction on the Shear Capacity of Reinforced Concrete Slabs Without Shear Reinforcement. PhD thesis, University of Southern Denmark. 299 p.

[21] Den Uijl, J. A., & Kaptijn, N. (2002). Structural consequences of ASR: An example on shear capacity. Heron, 47(2), 125–139.

[22] IStructE. (1992). Structural effects of alkali-silica reaction. Institution of Structural Engineers, London, UK. 48 p.

[23] Abe, M., Kikuta, S., Masuda, Y., & Tomozawa, F. (1989). Experimental study on mechanical behaviour of reinforced concrete members affected by alkali-aggregate reaction. Alkali-Aggreagte Reaction 8th International Conference, 691–696.

[24] Ahmed, T., Burley, E., & Rigden, S. (1998). The static and fatigue strength of reinforced concrete beams affected by alkali-silica reaction. ACI Materials Journal, 95(4), 376–387. https://doi.org/10.14359/380

[25] Smaoui, N. (2003). Contribution à l'évaluation du comportement structural des ouvrages d'art affectés de réaction alcalis-silice (ras).

[26] Inoue, S., Fujiii, M., Kobayashi, K., & Nakano, K. (1989). Structural behaviours of reinforced concrete beams affected by alkali-silica reaction. 8th International Conference on AAR in Concrete, 727–732.

[27] Bach, F., Thorsen, T. S., & Nielsen, M. P. (1993). Load-carrying capacity of structural members subjected to alkali-silica reactions. Construction and Building Materials, 7(2), 109–115.

[28] Deschenes, D., Bayrak, O., & Folliard, K. (2009). Shear capacity of large-scale bridge bent specimens subject to alkali-silica reaction and delayed ettringite formation. In ASCE (Ed.), Structures Congress 2009 (pp. 1049–1057).

[29] Grattan-Bellew, P. E., Cybanski, G., Fournier, B., & Mitchell, L. (2003). Proposed Universal Accelerated Test for Alkali-Aggregate Reaction The Concrete Microbar Test. Cement, Concrete, and Aggregates, 25(2), 29–34.